Optimization of Pinhole SPECT Calibration

Dirk Bequé, Johan Nuyts, Guy Bormans, Paul Suetens, and Patrick Dupont

***Abstract*— Previously, we developed a method to determine the acquisition geometry of a pinhole camera. This information is needed for the correct reconstruction of pinhole SPECT images. The method uses a calibration phantom consisting of three point sources. Their positions in the field of view influence the accuracy of the geometry estimate. This study proposes a specific configuration of point sources with a specific position in the field of view for optimal image reconstruction accuracy. For the proposed calibration setup, inaccuracies of the geometry estimate due to noise in the calibration data, only cause sub-resolution inaccuracies in reconstructed images. Further, the calibration method uses a model of the point source configuration, which is only known with limited accuracy. The study demonstrates however, that, with the proposed calibration setup, the error in reconstructed images is comparable to the error in the phantom model.**

***Index Terms*— Pinhole, geometric calibration, acquisition geometry, SPECT.**

I. Introduction

The reconstruction of pinhole SPECT data requires a correct description of the acquisition geometry of the pinhole camera. For a conventional pinhole system with a circular orbit of a plane detector, this geometry can be uniquely described by the seven parameters listed in Table I and extensively discussed in [1]. Previously, we developed a method to determine these parameters from the SPECT acquisition of a calibration phantom consisting of three point sources [1]. The method can be considered as an extension of previous methods, estimating a subset of the above parameters, using one [2]–[5] or two [6] point sources. To estimate all 7 parameters, three point sources are necessary and sufficient, and a model of the point source configuration has to be available [1]. For most point source configurations, the knowledge of at least two of the distances between the point sources provides a sufficient model [1]. In the methods practical implementation, all three distances between the point sources are taken into account in the phantom model [1].

The method first acquires a pinhole SPECT scan of the three point sources and calculates the mass centers of their projections. The acquisition geometry is then determined by a least squares fit of estimated point source projection locations to the measured mass centers. Besides the 7 parameters of the acquisition geometry, the positions of the point sources are estimated as well, but not the distances between them. This implies that the configuration of the calibration phantom has to be known (to be used as the phantom model), but not its position in the field of view of the camera.

TABLE I

PINHOLE PARAMETERS.

Symbol	Name
f	Focal length
d	Distance d
m	Mechanical offset
e_u	Electrical shifts
e_v	
Φ	Tilt angle
Ψ	Twist angle

With noisy calibration data, the acquisition geometry can only be estimated with limited accuracy. Both the configuration of the calibration phantom and its position in the field of view influence this accuracy. In the remainder of this text, the combination of phantom configuration and phantom position will be referred to as 'calibration setup'. The use of an incorrect phantom model in the calibration calculations can degrade this accuracy even further. During reconstruction, the resulting errors on the acquisition geometry propagate into the reconstructed images, causing loss of spatial resolution and/or image deformation. The aim of this study is to determine the optimal calibration setup for accurate image reconstruction and to study the effect of an incorrect phantom model for this optimal calibration setup. For clarity, table II provides an overview of the different entities involved in the calibration process.

II. Method

First, the propagation of noise on the calibration data to errors on the acquisition geometry is calculated by a linear approach. The propagation of phantom model errors is estimated by simulation. Then the effect on image reconstruction of the resulting estimation errors, due to either noisy data or phantom model errors, is evaluated.

A. Estimation Accuracy

The projection coordinates U_0 of the three calibration point sources can be calculated analytically in function of the acquisition geometry and the point source locations (calibration setup) [1]. For small variations ΔP in the acquisition geometry and/or phantom position, we assume that the resulting projection coordinates U can also be approximated from the original projections by a linear system

$$U = U_0 + M\,\Delta P. \tag{1}$$

Work supported by K.U.Leuven grant OT-00/32, F.W.O. grant G.0174.03 and K.U.Leuven grant IDO/02/012.

D. Bequé, J. Nuyts and P. Dupont are with the Dept. of Nuclear Medicine, K.U.Leuven, G. Bormans is with the Lab. for Radiopharmaceutical Chemistry, K.U.Leuven, and P. Suetens is with the Lab. for Medical Image Computing, K.U.Leuven.

(e-mail: dirk.beque@uz.kuleuven.ac.be)

TABLE II
CALIBRATION ENTITIES.

Name	# Parameters	Description
Acquisition geometry	7	Geometry of the pinhole system: $f, d, m, e_u, e_v, \Phi, \Psi$.
Phantom configuration	3	Actual distances between the 3 calibration point sources.
Phantom model	3	Values of the distances between the 3 point sources used in the calculations.
Phantom position	6	Actual position & orientation of the phantom in the field of view.
Calibration setup	9	Phantom configuration + Phantom position.

Here, M is a matrix containing the first order derivatives of the projection coordinates U to the parameters P. It is evaluated in the original acquisition geometry and phantom position, which yield the projections U_0. With $\Delta U = U - U_0$, (1) can be rewritten as

$$\Delta P = (M^T M)^{-1} M^T \Delta U. \tag{2}$$

Expressed in this way, the equation allows to calculate differences in the parameter estimates ΔP, due to specific changes of the projection coordinates ΔU. Noise on the projection coordinates causes such differences ΔU. This noise is however better characterized by its covariance matrix $\mathrm{cov}(U)$ than by a single noise realization ΔU. The covariance matrix $\mathrm{cov}(U)$ is propagated through the linear estimator of (2), yielding the covariance matrix $\mathrm{cov}(P)$ of the estimated parameters P

$$\mathrm{cov}(P) = (M^T M)^{-1} M^T \mathrm{cov}(U)\, M (M^T M)^{-1}. \tag{3}$$

The covariance matrix $\mathrm{cov}(P)$ provides an excellent measure of the noise on the estimated parameters. The evaluation of the reconstruction accuracy in the next section, uses however specific differences ΔP, instead of a covariance matrix $\mathrm{cov}(P)$. If all parameter errors were independent (zero covariances), an alternative would be to evaluate the effects of each parameter error (standard deviation) individually. By assuming independent errors on the point source projections ($\mathrm{cov}(U)$ is diagonal), a similar approach can here be followed: a set of independent combinations of errors is calculated and the effect on image reconstruction is then evaluated for each combination individually. The independent combinations ΔP can be found by a kind of decomposition of the covariance matrix. This section just demonstrates this decomposition on a small 3x3 covariance matrix, while appendix I presents a justification of this approach.

Consider the small 3x3 covariance matrix $\mathrm{cov}(P)$

$$\mathrm{cov}(P) = \begin{bmatrix} \sigma_{xx} & \sigma_{xy} & \sigma_{xz} \\ \sigma_{xy} & \sigma_{yy} & \sigma_{yz} \\ \sigma_{xz} & \sigma_{yz} & \sigma_{zz} \end{bmatrix}. \tag{4}$$

The first combination of errors ΔP_1 is calculated as a combination with the error of x equal to twice its standard deviation

$$\Delta P_1 = \begin{bmatrix} 2\sqrt{\sigma_{xx}} \\ 2\alpha\sqrt{\sigma_{xx}} \\ 2\beta\sqrt{\sigma_{xx}} \end{bmatrix} \text{with} \begin{cases} \alpha &= \frac{\sigma_{xy}}{\sigma_{xx}} \\ \beta &= \frac{\sigma_{xz}}{\sigma_{xx}} \end{cases}. \tag{5}$$

To calculate the other combinations of errors, the covariance matrix $\mathrm{cov}(P)$ is then changed to $\mathrm{cov}(P_1)$

$$\mathrm{cov}(P_1) = \begin{bmatrix} 0 & 0 & 0 \\ 0 & \sigma_{yy} - \alpha^2\sigma_{xx} & \sigma_{yz} - \alpha\beta\sigma_{xx} \\ 0 & \sigma_{yz} - \alpha\beta\sigma_{xx} & \sigma_{zz} - \beta^2\sigma_{xx} \end{bmatrix}. \tag{6}$$

with α and β as in (5). In this matrix, the variance of x has been eliminated and the variances of y and z have been reduced with the appropriate amount, according to their covariances with the parameter x. The covariance σ_{yz} has also been adapted to the new values of the variances of y and z. The above procedure is now repeated for the other diagonal elements, until all variances have vanished.

For errors in the phantom model, the parameter estimation accuracy is estimated by calibration simulations, since no sufficiently accurate linear system was found.

B. Reconstruction Accuracy

The reconstruction accuracy is evaluated for both loss of resolution and deformation of the reconstructed images. If a point source is reconstructed from its pinhole projections using the correct acquisition geometry, all projection rays intersect at the correct point in the field of view. With an incorrect acquisition geometry, we assume that the point source will be reconstructed at the point that is closest to all projection rays in a least squares way. The distances from that point to the projection rays are decomposed into three orthogonal components and either the maximum value or the root mean square of each component is used as a measure of the loss of spatial resolution. The image deformation due to the incorrect acquisition geometry is further calculated by 'reconstructing' a grid of point sources. After correction for a global translation and rotation of the reconstructed image, the remaining displacements of the reconstructed point sources reflect the image deformation. The displacements are again decomposed into three orthogonal components. For convenience, these point source displacements will further be referred to as 'image deformation'.

For a set of independent combinations of parameter estimate errors $\Delta P_1, \Delta P_2, ...$, obtained from the decomposition of a covariance matrix $\mathrm{cov}(P)$, this procedure is applied to each set individually and the results are quadratically added. This approach is based on the assumption that the uncorrelated sets of errors each have an independent effect on the image reconstruction accuracy.

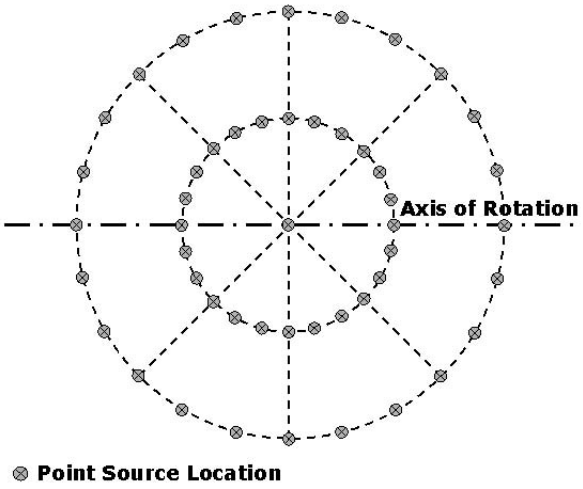

Fig. 1. Cross-section of the spherical grid of possible point source locations in the field of view. The complete grid is obtained by rotating the displayed grid over 0, 45, 90 and 135 degree about the rotation axis.

III. Experiments

A. Calibration Setup

This first experiment evaluates the effect of the calibration setup on the estimation and reconstruction accuracy. The aim is to find a calibration setup for optimal reconstruction accuracy. It can be shown that the field of view of a regular pinhole SPECT camera, can be well approximated by a sphere. The three calibration point sources can be positioned anywhere within this sphere, yielding a specific calibration setup. In this experiment, the positions of these point sources are systematically varied over the nodes of a spherical grid, to cover all possible calibration setups. Figure 1 shows a cross-section of this spherical grid, with the rotation axis of the pinhole camera indicated. The complete grid is obtained by rotating the grid shown in the image over 0, 45, 90 and 135 degree about the rotation axis. The outside of the grid corresponds with the edge of the (spherical) field of view. For each calibration setup obtained in this way, the estimation and reconstruction accuracy is calculated as described in section II.

The experiment is conducted for a pinhole camera with 24 cm focal length f. The focal point is rotating at 4 cm distance d around the rotation axis and the pinhole collimator has a 60 deg acceptance angle α. The parameters m, e_u, e_v, Φ and Ψ are all equal to zero, simulating an 'ideal' pinhole system. This acquisition geometry yields a field of view of 4 cm in diameter. The noise on the point source projection locations is Gaussian noise with 0.3 mm standard deviation. This is visually worse than the noise of real calibration measurements with the above acquisition geometry. To evaluate the image deformation part of the reconstruction accuracy, a grid of 7 seven coplanar point sources was used, as shown in Figure 2. This coplanar phantom provides sufficient information, because the circular orbit of the pinhole camera causes circular symmetry of the reconstruction properties, with respect to the axis of rotation.

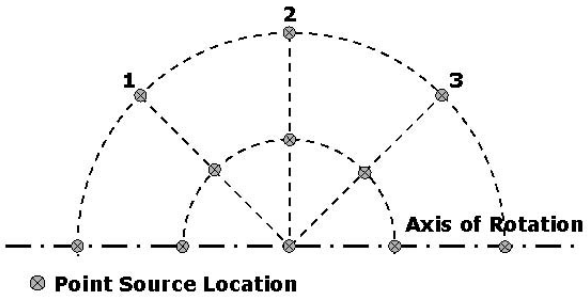

Fig. 2. Grid of point sources to evaluate the deformation of reconstructed images. The numbers 1, 2 and 3 indicate a relationship of those point sources with the calibration point sources of Figure 3.

B. Incorrect Phantom Model

This experiment evaluates the effect of errors in the calibration phantom model on the estimation and reconstruction accuracy for the optimal calibration setup of the first experiment, shown in Figure 3. First the correct, noiseless projection data of the calibration point sources are calculated. Then the calibration point sources of the optimal setup are randomly displaced in three orthogonal directions with a normal distribution of 0.1 mm standard deviation. This modified setup is used to calculate the calibration phantom model, so that it contains modelling errors. It is then used in the calibration procedure in combination with the correct phantom projection data. This calibration yields a set of incorrect acquisition parameter estimates and the effect of these inaccuracies on the reconstruction accuracy is further evaluated as discussed in section II.B. The procedure is performed for 250 random modifications of the original optimal calibration setup and for the same pinhole camera geometry as in the first experiment.

IV. Results

A. Calibration Setup

Different calibration setups optimize the accuracy of different acquisition parameter estimates and no solution was found minimizing the errors on all parameters simultaneously. However, a large number of setups can be found, yielding maximum image deformation and maximum loss of spatial resolution of less than 0.05 mm, while the attainable image resolution is expected to be 0.5 mm or higher. As these errors are much smaller than the attainable resolution, each of these setups can be considered to be equally favorable. The solution shown in Figure 3 was nevertheless singled out, because it also strongly reduces the standard deviation of each of the acquisition parameter estimates. It is a triangular configuration of point sources with the rotation axis of the camera in the plane of the triangle and with each of the point sources at the edge of the field of view. Table III shows the standard deviations of each of the 7 acquisition parameter estimates. The values $\sigma_{\min}$ indicate the minimum standard deviation found for that particular parameter during the experiment: the standard deviations of different parameters can be obtained from different calibration setups. The values σ_{opt}

TABLE III

	f [mm]	d [mm]	m [mm]	e_u [mm]	e_v [mm]	Φ [deg]	Ψ [deg]
$\sigma_{\min}$	0.20	0.03	0.03	0.22	0.19	0.04	0.01
σ_{opt}	0.21	0.03	0.03	0.23	0.19	0.04	0.01
σ_{conf}	0.22	0.03	0.03	0.23	0.20	0.04	0.01

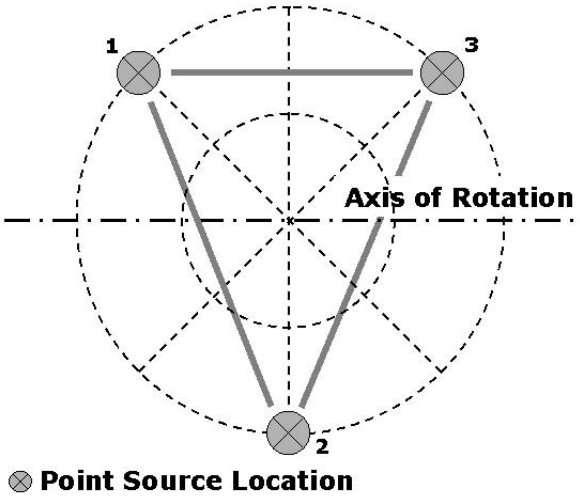

Fig. 3. Optimal Calibration Setup. The numbers 1, 2 and 3 indicate a relationship of the calibration point sources with specific point sources of the point source grid of Figure (2)

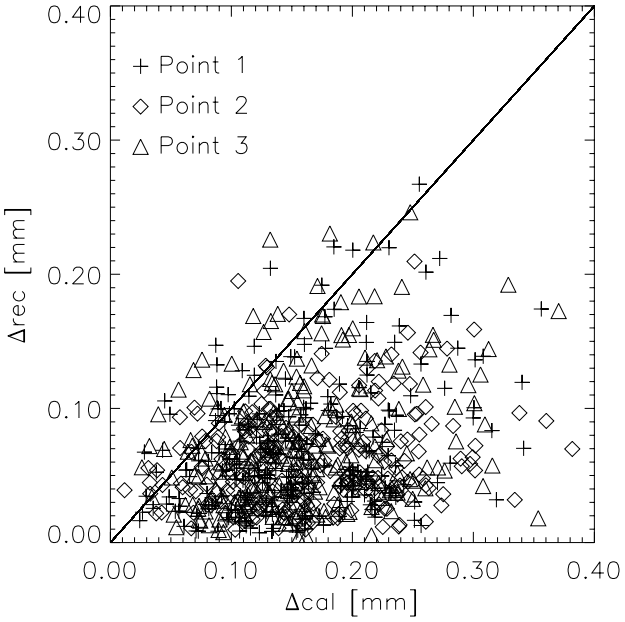

Fig. 4. Displacements Δ_{rec} of the reconstructed point sources versus the displacements of the calibration model with respect to the phantom configuration Δ_{cal}.

are the standard deviations obtained with the optimal calibration setup of Figure 3 and they are all very close to the minimum standard deviations $\sigma_{\min}$.

The linear system assumption of section II.A was finally verified for the optimal calibration setup, by a simulation experiment using 250 noise realizations of the correct point source projection data. This experiment yielded the standard deviations σ_{conf} in table III and is in excellent agreement with the linear approximation.

B. Incorrect Phantom Model

The effect of an incorrect phantom model on the estimation accuracy differs for the different parameters. The parameter estimates of the mechanical offset m, the electrical shift e_u and the twist angle Ψ, are hardly affected by the inaccuracies of the model. The standard deviations of the other parameters are however large in comparison with those obtained in the first experiment, especially those of the electrical shift e_v and the tilt angle Φ. Table IV shows the above standard deviations σ_{exp2}.

The image deformations due to the incorrect phantom models are of the same magnitude as the deformation of the phantom

TABLE IV

	f [mm]	d [mm]	m [mm]	e_u [mm]	e_v [mm]	Φ [deg]	Ψ [deg]
σ_{exp2}	0.53	0.13	0.00	0.02	2.93	0.70	0.00

model itself with respect to the correct phantom configuration. Further, the point sources 1, 2 and 3 of the point source grid of Figure 2 have a special relationship with the calibration point sources. Keeping in mind the circular symmetry of the reconstruction properties, each of them can be thought of to be located at the same place in the field of view as the corresponding calibration point source. The displacements Δ_{rec} of their reconstructions (image deformation) are compared in Figure 4 with the displacements Δ_{cal} made in the phantom modelling step of this experiment. It shows that the image deformation Δ_{rec} is generally less than the modelling errors Δ_{cal}. The sum of the displacements of the 3 reconstructed point sources is always less than the sum of the modelling errors.

The resolution degradation is limited to 0.05 mm or less and is again negligible in comparison with the expected resolution.

V. Discussion

The method we developed to determine the acquisition geometry of a pinhole camera [1], is based on the assumption that the calibration phantom is the representation of an image, which can be thought of as an infinite collection of point sources. Stated in this way, the best calibration phantom, is the one best representing the entire image. From this point of view, the best way to improve the phantom clearly consists in adding additional point sources to it. It also suggests that the point sources should be distributed to cover the entire field of view, although not necessarily in a uniform way. Our results indicate that the theoretically minimal number of point sources [1], placed at well chosen locations in the field of view, is

already sufficient for practical purposes. The above concept also explains how the use of an incorrect phantom model, results in an equivalent deformation of the reconstructed image. The calibration minimizes the inconsistency between the fixed, but incorrect phantom model and the measured projections by modifying the projector. During reconstruction, the same projector is then used to generate an image, which is consistent with its projections.

The optimal calibration setup also seems to agree with earlier findings of Wang *et al.* [4] and Noo *et al.* [6] about optimal setups for their calibration methods. Wang *et al.* [4] used a single calibration point source and reported that the estimation accuracy improved with larger distances between the point source and the axis of rotation. On the other hand, Noo *et al.* [6] used two point sources and reported that these point sources should be placed well apart from each other and from the focal plane, with the focal plane being the plane in which the focal point is rotating during image acquisition. In the optimal calibration setup, the point sources are all located on the edge of the field of view, yielding the best compromise in distance to the axis of rotation and distance to the focal plane for a spherical field of view. Calibration point source 2 is located exactly in the focal plane, but at the largest possible distance from the rotation axis. The point sources 1 and 3 on the other hand, are located at a considerable distance from the focal plane, but without sacrificing too much of their distance to the rotation axis.

As mentioned before, the optimal calibration setup of figure 3 was optimized to yield very low variances of the acquisition parameter estimates with the best possible reconstruction accuracy, for calibrations with noisy calibration data. This setup was then evaluated for inaccuracies in the phantom model, but not optimized. Optimizing the phantom for a combination of noisy data and phantom model errors can result in a different optimal calibration setup. This setup will then depend on the relative magnitudes of the noise on the data and the errors in the phantom model. However, for a fixed phantom configuration, the distances between the point sources need only to be measured once. We assume that these distances are then measured with sufficient accuracy. The second simulation experiment relates the desired reconstruction accuracy to the required phantom model accuracy. On the other hand, inaccuracies due to noise can only be diminished by a higher activity in the calibration point sources or longer calibration scan times. Both solutions are undesirable for frequent camera calibrations.

VI. Conclusion

A specific configuration of three point sources with a specific position and orientation in the field of view has been proposed as a pinhole SPECT calibration setup. This setup yields optimal results for both the accuracy of the estimated pinhole acquisition geometry and the accuracy of image reconstruction, when calibrating with noisy calibration data sets. With the proposed calibration setup, errors in the phantom model cause image deformations of the same magnitude or less.

Appendix I
Covariance Matrix Decomposition

The approach of Section II.A to decompose the covariance matrix, actually consists in modifying the covariance matrix into a larger block-diagonal matrix. This is done by splitting the original parameters up into a sum of different terms which are correlated with specific terms from the other parameters. With $N = (M^T M)^{-1} M^T$, and P consisting of three parameters x, y and z, (2) can be written as,

$$\Delta x = \sum_{i=1}^{m} n_{ix} \Delta u_i, \tag{7}$$

$$\begin{aligned} \Delta y &= \alpha \sum_{i=1}^{m} n_{ix} \Delta u_i + \sum_{i=1}^{m} (n_{iy} - \alpha n_{ix}) \Delta u_i \\ &= \Delta y' + \Delta y'' \end{aligned} \tag{8}$$

$$\begin{aligned} \Delta z &= \beta \sum_{i=1}^{m} n_{ix} \Delta u_i + \sum_{i=1}^{m} (n_{iz} - \beta n_{ix}) \Delta u_i \\ &= \Delta z' + \Delta z'' \end{aligned} \tag{9}$$

with u_i $i = 1, 2, ..., m$ the elements of ΔU and n_{ix} the elements of the x-row of N. With cov(U) being a diagonal matrix and with α and β like in (5), it can be shown that y' and z' are perfectly correlated with each other and with x, while they show no correlation (zero covariance) with y'' and z''. Thereby, splitting the parameters y and z up yields a 5x5 covariance matrix consisting of two blocks. The first block is formed by the perfectly correlated parameters x, y' and z', and the other 2x2 block is formed by y'' and z'' and is equal to the lower block in (6). Because the parameters of the first block are perfectly correlated, they can be treated like a single parameter.

References

[1] D. Bequé, J. Nuyts, G. Bormans, P. Suetens, and P. Dupont, "Characterization of Pinhole SPECT Acquisition Geometry, " *IEEE Trans. Med. Imag.*, Vol. 22, No. 5, pp. 599-612.

[2] G. T. Gullberg, B. M. W. Tsui, C. R. Crawford, J. G. Ballard, and J. T. Hagius, "Estimation of geometrical parameters and collimator evaluation for cone beam tomography," *Med. Phys.*, vol. 17(2), pp. 264–272, 1990.

[3] J. Li, R. J. Jaszczak, H. Wang, K. L. Greer and, R. E. Coleman, "Determination of both mechanical and electronic shifts in cone beam SPECT," *Phys. Med. Biol.*, vol. 39, pp. 743–754, 1993.

[4] H. Wang, M. F. Smith, C. D. Stone, and R. J. Jaszczak, "Astigmatic single photon emission computed tomography imaging with a displaced center of rotation," *Med. Phys.*, vol. 25(8), pp. 1493–1501, 1998.

[5] Ph. Rizo, P. Grangeat, and R. Guillemaud, "Geometric Calibration Method for Multiple-Head Cone-Beam SPECT System," *IEEE Trans. Nucl. Sci.*, vol. NS-41(6), pp. 2748–2757, 1994.

[6] F. Noo, R. Clackdoyle, C. Mennessier, T. A. White, and T. J. Roney, "Analytic method based on identification of ellipse parameters for scanner calibration in cone-beam tomography," *Phys. Med. Biol.*, vol. 45, pp. 3489–3508, 2000.